DOI 10.1007/s10946-022-10048-z
Journal of Russian Laser Research, Volume 43, Number 2, March, 2022

TWO-STAGE INCREMENTAL THREE-DIMENSIONAL SPATIAL MAPPING APPROACH USING A SINGLE-LAYER LIDAR

Shifeng Wang,[1,2] Zhiwei Wang,[1*] Jiahang Lyu,[1] Yuan Zhou,[1] Jin Meng,[1] and Long Hu[1]

[1] *School of Optoelectronic Engineering, Changchun University of Science and Technology National Demonstration Center for Experimental Opto-Electronic Engineering Education Weixing Road 7089, Changchun City 130022, Jilin Province, China*

[2] *Key Laboratory of Optoelectronic Measurement and Optical Information Transmission Technology Changchun University of Science and Technology Weixing Road 7089, Changchun City 130022, Jilin Province, China*

*Corresponding author e-mail: wangzhiwei8077@163.com

Abstract

Multilayer-lidar-used solution is popular though financial consumption is extremely expensive. In addition, multilayer lidars are barely able to reconstruct an incremental three-dimensional (3D) spatial mapping, due to the limited pitch-angler movement. To solve this problem, in this paper we design and develop a device employed a low budget single-layer lidar and a stepping motor. Spatial coordinate algorithm converts single-layer lidar data from polar coordinates to Cartesian coordinates (3D). Then the converted point cloud data is processed in two stage. In the first stage, the converted 3D data is coarse registered by the SAC-IA algorithm to obtain a better initial pose. In the second stage, the ICP algorithm is used to accurately register the point cloud data to reconstruct the incremental 3D spatial mapping. The experiments performed show that the single-layer lidar used spatial mapping by the two-stage method senses more complete space than that of using 16-layer lidar. The quantitative analysis of the incremental 3D spatial mapping experiments show that the accuracy (0.0998) meets the engineering requirements. Moreover, the lower cost (40% off) is also an advantage for low budget applications.

Keywords: single-layer lidar, spatial coordinate algorithm, 3D spatial mapping, SAC-IA algorithm.

1. Introduction

At present, there are two main methods of 3D mapping. One is vision based and the other is lidar based. For example, Lijun Qi et al. shoot the same scene at different shooting positions with the binocular vision measurement principle and build a 3D model based on the visual difference between the two images [1]. Pire et al. proposed a classic Binocular Stereo Vision SLAM algorithm called S-PTAM system [2]. The system follows a parallel tracking and mapping strategy, and the tracking thread estimates the camera pose at the frame rate. However, this method requires exact intensity of light and is susceptible to light, which leads to instability. Henry et al. proposed a method using Kinect-style depth cameras for dense 3D modeling [3]. Their experiments showed higher accuracy for building construction and demonstrated its feasible application for economical gaming and entertainment, but problems like

Manuscript submitted by the authors in English on May 16, 2021.

limited lighting repetitive structures and lack of distinctive feature have not been solved. Bingjie Wang proposed a chaotic lidar for underwater ranging and three-dimension (3D) imaging applications [4].

In 2019, a novel method using a single-layer lidar and an inertial measurement unit (IMU) was proposed [5]. This is expected to replace the multiple-layer lidar in perceiving surrounding environment. The cost of the design is relatively low. However, there will be unavoidable errors, and 3D mapping cannot be completed when data from two sensors are fused. According to this limitation, in this paper, we design an algorithm to replace IMU by using spatial coordinate transformation, so as to reduce the error caused by data fusion. In this paper, we design an algorithm to replace IMU with space coordinate conversion to reduce the error caused by data fusion. It further processes the point cloud data to get better results based on the traditional ICP registration algorithm, so as to complete 360° all-round 3D mapping.

2. Design Approach and Experimental Methodology

2.1. Experimental Platform

In this design, the UTM-30LX single-layer lidar is fixed on the rotating shaft of the stepper motor. In Fig. 1, we present the design of the scanning lidar. The single-layer lidar continuously rotates clockwise in the XOY horizontal plane with the Z axis as the rotation axis; see Fig. 1 a. The α in Fig. 1 b is the angle between two adjacent scans. The radial lines display the scanning beam of the single-layer lidar.

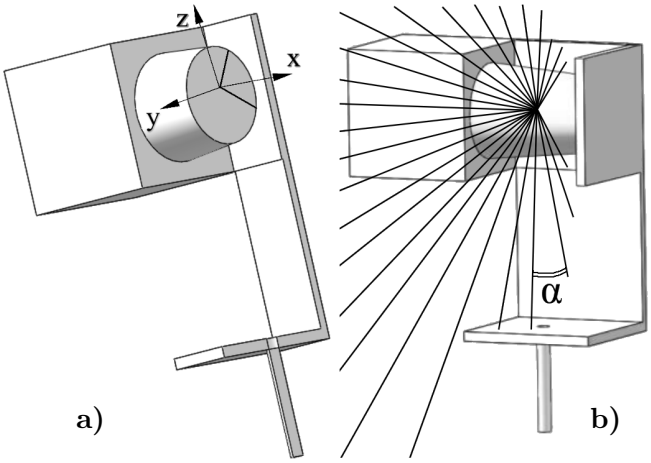

Fig. 1. Mechanical structure.

Fig. 2. Experimental installation.

The device is mainly composed of the single-layer lidar, a STM32 microcontroller, stepper motor, and power supply; see Fig. 2.

The single-layer lidar has a measuring angle range of 270 ° and 1081 points per scan of data. In Fig. 3, we show the scanned area of the lidar, and the performance parameters of the single-layer lidar are shown in Table 1.

2.2. Spatial Coordinate Algorithm

Let $n^{'}$ ($n^{'} = 1081$) be the points received in a lidar scan and each scan time as S_1 ($S_1 = 25$ ms). Let ρ be the measured distance data. The time of circular rotation for single-layer lidar is S_2 ($S_2 = 3000$ ms).

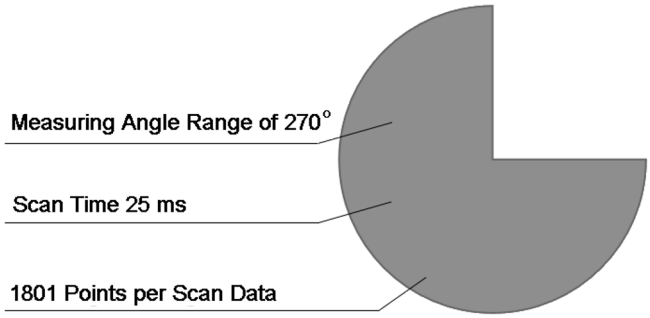

Fig. 3. Diagram of the scanned area.

Table 1. Working Parameters Used in This Work.

Performance Parameters	UTM-30LX
Accuracy at 0.1 to 10 m	±30 mm
Accuracy at 10 to 30 m	±50 mm
Scan frequency	40 Hz
Voltage	12.0 V DC ±10%
Operating Temperature	−10 to 50°C

Let α be the angle that between two adjacent beams of the single-layer lidar,

$$\alpha = 270^{\circ}/n^{'}. \tag{1}$$

Time interval of each point emitted by the single-layer lidar can be denoted as

$$c = S_1/n^{'}. \tag{2}$$

The single-layer lidar rotates b within the time c,

$$b = 360^{\circ} \times c/S_2. \tag{3}$$

As shown in Fig. 1, the angle between the first beam from the lidar and the negative y axis is $\pi/4$. Thus, the Cartesian coordinates can be calculated out by (4),

$$\begin{cases} x = 0, \\ y = -\rho \cdot \cos(\pi/4), \\ z = \rho \cdot \sin(\pi/4). \end{cases} \tag{4}$$

By analogy, the coordinate equation of the lidar rotation can be obtained, using the notation ρ_i ($i = 1, 2, 3 \cdots 32430$) being the distance collected by the lidar so that, when $n_i < 182$ and $m_i < 32430$; $n_i = 1, 2, 3 \ldots 1081$; $m_i = 1, 2, 3 \ldots 32430$, it reads

$$\begin{cases} x = \rho_i \cdot \cos\left[(45^{\circ}\pi/180^{\circ}) + (n_i - 1) \cdot \alpha\right] \cdot \sin(m_i b), \\ y = -\rho_i \cdot \cos\left[(45^{\circ}\pi/180^{\circ}) + (n_i - 1) \cdot \alpha\right] \cdot \cos(m_i b), \\ z = \rho_i \cdot \sin\left[(45^{\circ}\pi/180^{\circ}) + (n_i - 1) \cdot \alpha\right]. \end{cases} \tag{5}$$

When $181 < n_i < 542$ and $m_i < 32430$,

$$\begin{cases} x = -\rho_i \cdot \cos\left[(135^{\circ}\pi/180^{\circ}) - (n_i - 1) \cdot \alpha\right] \cdot \sin(m_i b), \\ y = \rho_i \cdot \cos\left[(135^{\circ}\pi/180^{\circ}) - (n_i - 1) \cdot \alpha\right] \cdot \cos(m_i b), \\ z = \rho_i \cdot \sin\left[(135^{\circ}\pi/180^{\circ}) - (n_i - 1) \cdot \alpha\right]. \end{cases} \tag{6}$$

When $541 < n_i < 902$ and $m_i < 32430$,

$$\begin{cases} x = -\rho_i \cdot \cos\left[(n_i - 1)\alpha - (135^{\circ}\pi/180^{\circ})\right] \cdot \sin(m_i b), \\ y = \rho_i \cdot \cos\left[(n_i - 1)\alpha - (135^{\circ}\pi/180^{\circ})\right] \cdot \cos(m_i b), \\ z = -\rho_i \cdot \sin\left[(n_i - 1)\alpha - (135^{\circ}\pi/180^{\circ})\right]. \end{cases} \tag{7}$$

When $901 < n_i < 1082$ and $m_i < 32430$,

$$\begin{cases} x = \rho_i \cdot \cos\left[(315^\circ\pi/180^\circ) - (n_i - 1)\alpha\right] \cdot \sin(m_i b), \\ y = -\rho_i \cdot \cos\left[(315^\circ\pi/180^\circ) - (n_i - 1)\alpha\right] \cdot \cos(m_i b), \\ z = -\rho_i \cdot \sin\left[(315^\circ\pi/180^\circ) - (n_i - 1)\alpha\right]. \end{cases} \tag{8}$$

The n_i return to the initial value when the $n_i = 1081$. The calculation stops until $m_i = 32430$. By analogy, the point cloud space Cartesian coordinates of the lidar rotating to other angles can be calculated. Let the collected data by the single-layer lidar be logged as a frame of point cloud data when the motor rotates 360°.

2.3. SAC-IA Algorithm

Sample consensus initial alignment (SAC-IA) is based on the corresponding relationship between the fast point features histograms (FPFH) to complete the initial registration. Let P be a frame of point cloud data. It selects n sampling points from the frame of point cloud P. It makes the sampled points have as many FPFH features as possible. The threshold d is set in advance so that the distance between the sampling points is larger than d. Traverse the points in the other frame of point cloud data Q to find any point cloud data with similar FPFH features in the previous frame data P. The found point cloud has a one-to-one correspondence with the point cloud data in the point cloud P. Afterwards, the rigid transform matrix between corresponding points can be calculated. The "sum of distance error" function is used to judge the performance of the current registration transformation; the function is mostly expressed by Huber penalty function,

$$\sum_{i=1}^{n} H(l_i) \begin{cases} \dfrac{1}{2} l_i^2, & |l_i| < m_l, \\ \dfrac{1}{2} m_l(2|l_i| - m_l), & |l_i| > m_l. \end{cases} \tag{9}$$

Here, m_l is the set value, l_i is the distance difference of the ith frame of pairwise corresponding points after rigid transformation. Calculate the value of "sum of distance error" function after each rigid transformation. The transformation matrix is the final registration transformation matrix when the value is the smallest.

2.4. ICP Registration Algorithm

The current method of point cloud registration is mostly iterative closest point [6]. The point cloud Q is registered to the Cartesian coordinate system of the point cloud P [7]. The central idea of ICP algorithm is the optimum registration method based on least-square method. The algorithm is to rotate and pan the point cloud Q, find the best rotation matrix R and translation transformation T, and optimally match the point cloud Q with the point cloud P in the same Cartesian coordinate system. According to the above introduction, $P = \{p_1 \dots p_n\}$ refers the point cloud P, while $Q = \{q_1 \dots q_n\}$ refers the point cloud Q,

$$e_i = p_i - R \times q_i + T. \tag{10}$$

The least-squares problem is established; here, R and T are the lowest value that can make the sum of squares error,

$$\min J = 1/2 \times \sum_{i=1}^{n} \|p_i - (R \times q_i + T)\|^2 . \tag{11}$$

According to R and T, we can register the point cloud P with the point cloud Q.

2.5. Evaluation Algorithm of Incremental 3D Spatial Mapping

Equation (11) can accurately reflect the accuracy of incremental 3D spatial mapping (3D spatial map increases with the recorded data). Since the single-layer lidar obtains point cloud data through rotation of 360°, it can be assumed that the data of the first scan and last scan are theoretically completely coincident. The algorithm calculates the sum of the Euclidean distance between the corresponding points in the two frames of data and divides it by the total number of point clouds scanned once to obtain the value of the average distance. Let S be the evaluation score and g_i, the data from the first scan. Also f_i is the data from the last scan, g_i is the closest point to f_i, and $n = 1081$ is the number of point cloud data in a scan. Then we arrive at

$$S = \frac{\sum_{i=0}^{n} \|g_i - f_i\|}{n} . \tag{12}$$

3. Experiment

3.1. Experimental Platform

We reconstructed an incremental 3D spatial mapping of the hall using a single-layer lidar and a stepper motor system and compared it with the results of the 16-layer lidar. The experimental platform has a processor (CPU) at 3.7 GHz, 16 Gb RAM, discrete graphics card with 8 Gb RAM, Windows 10 operating system, and VS 2013 version configuration PCL environment.

3.2. Experimental Procedure and Results

In order to verify the results, the hall was selected as the experimental site; it is shown in Fig. 4.

According to Sec. 2.2, we can obtain the collected data by single-layer lidar. In this way, an incremental 3D spatial mapping of the whole hall can be constructed. We collect seventeen frames of date in the hall, and the distance data is converted into Cartesian space data through the spatial coordinate algorithm. One frame of point cloud date is shown in Fig. 5.

3.2.1. First Stage SAC-IA Registration

First of all, two frames of point cloud data were selected randomly from the collected 17 frames of point cloud data, and two frames of data can be registered in the same Cartesian coordinate system. When the initial position deviation of two frames data is large, and two frames data are only registered by the ICP, it tends to cause the problem of local optimum solution. In Fig. 6, we show the problem of local optimum solution.

Fig. 4. RGB picture of the experimental site.

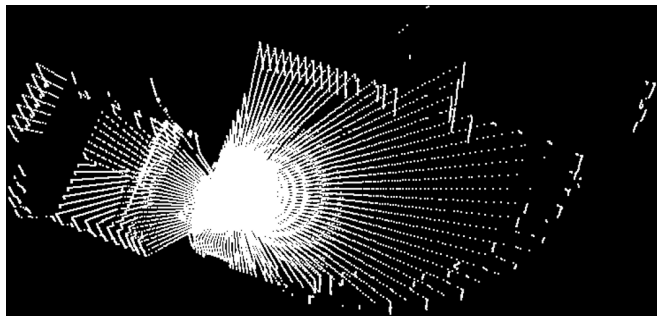

Fig. 5. One frame point cloud.

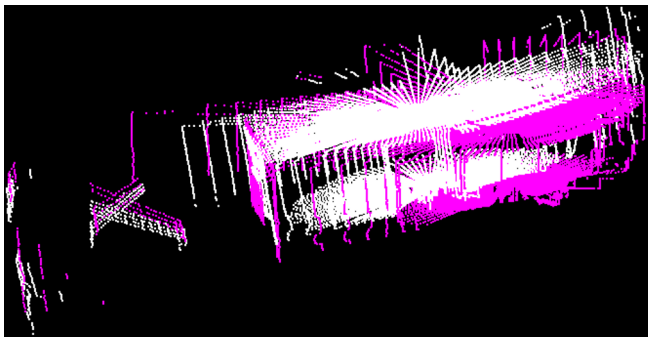

Fig. 6. Coarse registration effect.

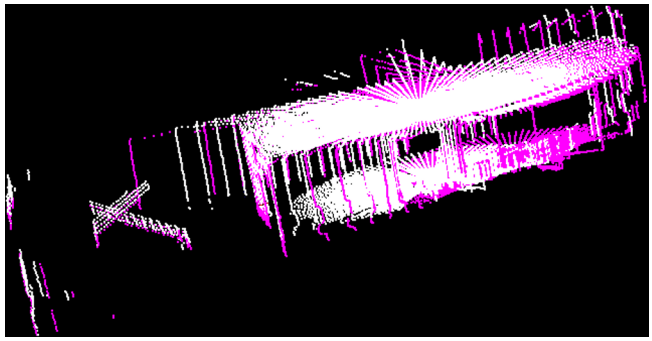

Fig. 7. Fine registration effect.

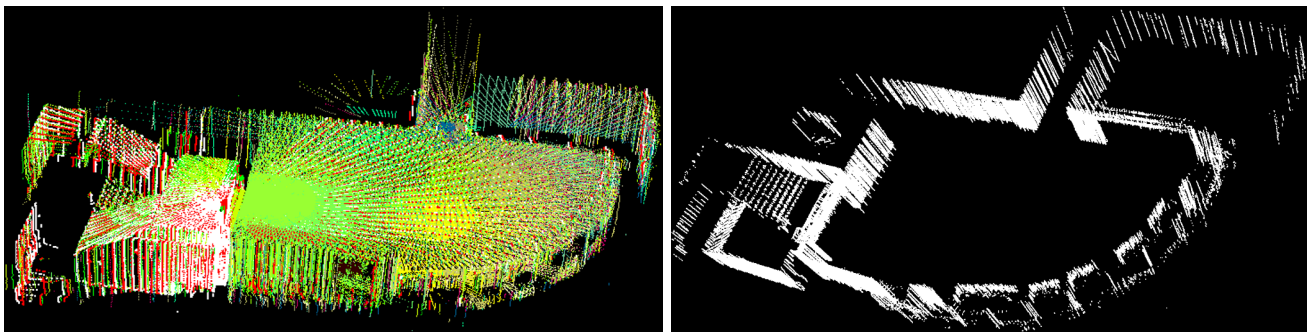

Fig. 8. Registration effect.

3.2.2. Second Stage ICP Registration

In the previous section, we obtained the point cloud data after SCA-IA coarse registration. One can see that the effect of registration is not good. Thus, ICP fine registration is carried out, and the effect after registration is shown in Fig. 7.

3.2.3. Experimental Results

Seventeen frames of point cloud data are registered with the two-step algorithm; the results are shown in Fig. 8, left. After removing the ground and ceiling points, the 3D spatial mapping of the hall interior is shown in Fig. 8, right.

Table 2. Accuracy Evaluation of Incremental 3D Spatial Mapping.

Number of Frames	1	2	3	4	5	6	7	8	9	Average
Score	0.118	0.0904	0.0936	0.0973	0.0133	0.0125	0.087	0.0926	0.0609	0.0998

Nine frames of data were randomly sampled from all the data, and the nine frames of data were reconstructed and scored. Calculate the average score of the reconstruction of each frame; it is considered that the average value is the final score of the whole incremental 3D spatial mapping. Table 2 shows that the score of the reconstruction algorithm is 0.0998; it completely meets the requirements for environmental exploration in some scenarios.

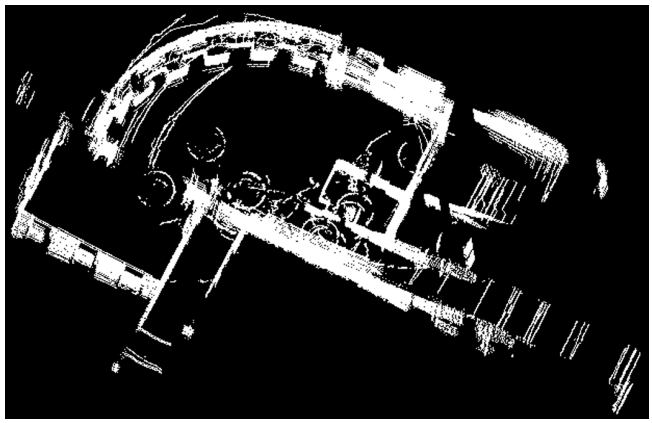

Fig. 9. Registration effect after removing the ground and ceiling points.

3.2.4. 16-Layer Lidar Reconstruction Incremental 3D Spatial Mapping

We use the same method to register the point cloud data collected by the 16-layer lidar in the hall. The results are shown in Fig. 9.

Comparing the registration effect of a single-layer lidar and 16-layer lidar, it is not difficult to find that the 16-layer lidar can only reconstruct part of the environment. This is caused by the small pitch angle range of the 16-layer lidar. The single-layer lidar is better than 16-layer lidar in terms of the integrity of the incremental 3D spatial mapping.

3.3. Comparison of Incremental 3D Spatial Mapping Details of Multilayer Lidar and Single-Layer Lidar

In Fig. 10 a, we see that there are more drift points at the connection between the wall and the ground reconstructed by the multilayer lidar; for example, the red point clouds are drifting point. Figure 10 demonstrates that the reconstruction effect of the single-layer lidar is significantly better than that of the multilayer lidar.

3.4. Cost Comparison

One can see from Table 3 that this equipment has obvious advantages in price compared with multilayer lidar.

Table 3. The Current Price Comparison of Various Sensors.

Device	Cost, USD
Single-layer lidar + stepper motor	4000
16-layer lidar	8000
32-layer lidar	40000

4. Conclusions

The method elaborated uses a structure that combines a single-layer lidar with a stepping motor, so that the single-layer lidar rotates clockwise around the Z axis in the horizontal direction to collect data. The spatial coordinate algorithm is used to convert the two-dimensional (2D) coordinates in the data into 3D coordinates. Then the two-stage registration algorithm (SAC-IA and ICP) is used to splice the transformed data to complete the incremental 3D spatial mapping of the hall.

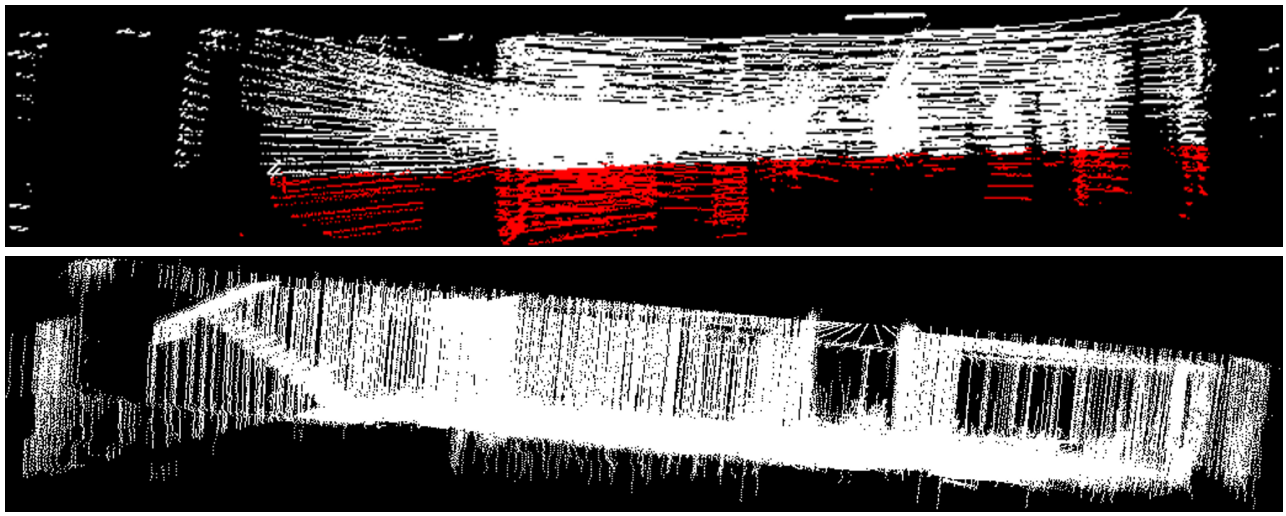

Fig. 10. Detailed comparison of 3D spatial mapping of the multilayer lidar (a) and the single-layer lidar (b).

The single-layer lidar has great advantages compared with the multilayer lidar. It has much lower cost than that of the multilayer lidar. In addition, the angle between two adjacent layer beams of multilayer lidar is 2°, while the angle of that in this approach is 0.25°, which leads to a higher density scan. In this design, SAC-IA coarse registration and ICP exact registration are used to reconstruct the incremental 3D spatial mapping, and the 3D spatial mapping results are quantitatively analyzed. The analysis shows that the accuracy on 3D spatial mapping of this design can meet the requirements for engineering 3D reconstruction.

In future work, more registration algorithms need to be tested using this method to find a better registration accuracy and a lower time consumption. At the same time, the experimental site can be change to outdoor. Therefore, it is imperative to improve the SAC-IA and ICP registration method to complete the incremental 3D spatial mapping of the outdoor scene.

Acknowledgments

This work is funded by Natural Science Foundation of Jilin Province under Grant No. 20150101047JC. This work is also supported by the 111 Project of China No. D17017 and OptoBot Lab, School of Optoelectronic Engineering, CUST.

References

1. L. J. Qi, "Research on 3D reconstruction technique based on uncalibrated camera binocular vision," MSc Theses, Harbin Institute of Technology, Harbin, China (2017).
2. T. A. N. Pire, T. Fischer, G. I. Castro, et al., *Rob. Autonom. Syst.*, **93**, 27 (2017); DOI: 10.1016/j.robot.2017.03.019
3. P. Henry, M. Krainin, E. Herbst, et al., *Int. J. Robotics Res.*, **31**, 647 (2012).
4. B. Wang, Z. Guo, Z. Shen, et al., *J. Russ. Laser Res.*, **41**, 399 (2020).
5. P. F. Zhang and S. F. Wang, *Lasers Eng.*, **42**, 187 (2019).
6. P. J. Besl and N. D. McKay, *IEEE Trans. Pattern Anal. Mach. Intell.*, **14**, 239 (1992).
7. F. Pomerleau, F. Colas, R. Siegwart, and S. Magnenat, *Auton. Robot.*, **34**, 133 (2013).